Electronic Supplementary Material (ESI) for Journal of Materials Chemistry A.

Insights into the Extraction of Photogenerated Holes from CdSe/CdS Nanorods for Oxidative Organic Catalysis

Yuchen Sha, [a, b] Xiao-Min Lin,[b, *] Jens Niklas, [c] Oleg G. Poluektov, [c] Benjamin T. Diroll, [b] Yulin Lin, [a, b] Jianguo Wen, [b] Zachary D. Hood,[d] Aiwen Lei, [a,*] and Elena V. Shevchenko [b,e*]

[a] Institute of Advanced Studies (IAS), College of Chemistry and Molecular Sciences, Wuhan University, Wuhan 430072, Hubei, P. R. China;

[b] Center for Nanoscale Materials. [c] Chemical Sciences and Engineering Division and [d] Applied Materials Division, Argonne National Laboratory, Argonne, Illinois, 60439 USA.

[e] Department of Chemistry and James Frank Institute, University of Chicago, Chicago, Illinois, 60637 USA.

*E-mails: Xiao-Min Lin (xmlin@anl.gov), Aiwen Lei (aiwenlei@whu.edu.cn), Elena Shevchenko (eshevchenko@anl.gov)

Supporting Information

1. Characterization of as-prepared CdSe/CdS nanorods

Powder x-ray diffraction measurement was carried out to identify the structure of as-prepared CdSe/CdS nanorods. The measurement was done using a Bruker D2 Phaser analytical x-ray system.

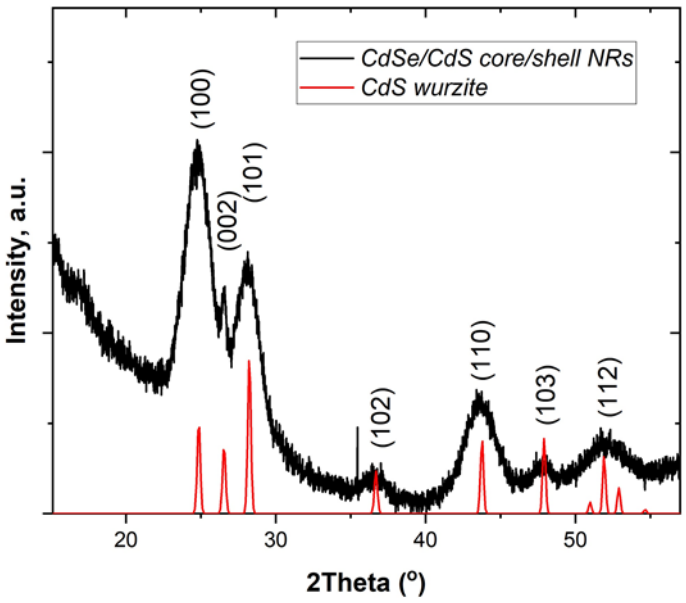

Fig. S1. The XRD pattern of CdSe/CdS core/shell nanorods (shown in black). The peaks shown in red correspond to wurtzite phase of CdS (https://icsd.fiz-karlsruhe.de/display/details.xhtml). The difference in the intensities of XRD patterns of CdSe/CdS nanorods and CdS reference are

due to preferential growth of {001} CdS facets[1] and preferred orientation of nanorods on the XRD substrate

X-ray photoelectron spectroscopy (XPS) spectra were collected for a powder sample on a Thermo K-Alpha XPS system with a spot size of 400 μm and a resolution of 0.1 eV. Samples were etched with Ar+ sputtering at a rate of 0.05 nm/sec. All spectra were processed using Thermo Avantage, which is a software package provided through ThermoScientific.

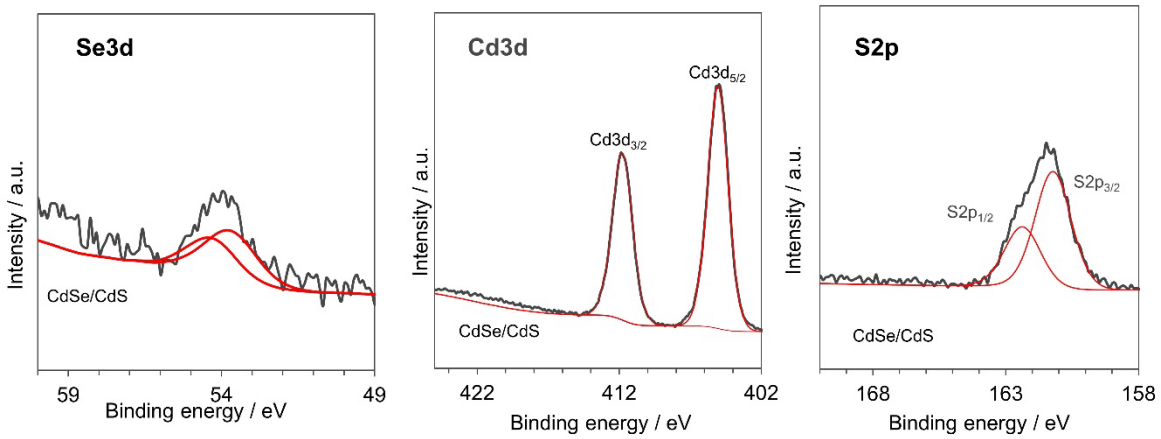

Fig. S2. XPS spectra at Se3d, Cd3d and S2p show that the as-prepared sample has metal sulfide feature. A weak signal of Se is a result of embedded CdSe core within the CdS nanorods.

2. Supporting TEM image of 113 nm long CdSe/CdS NRs

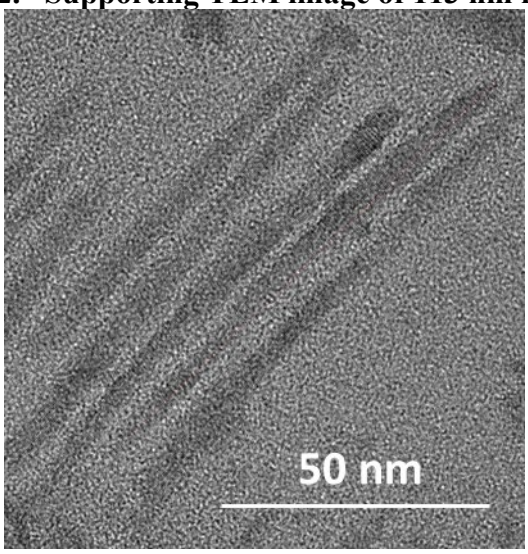

Fig. S3. TEM images of ~113 nm long CdSe/CdS NRs with 3.1 nm CdSe cores.[2]

3. Apparent Quantum Yield of the photooxidative reaction of thiophenol.

In order to determine the apparent quantum yield (APY) of the photooxidative reaction of thiophenol, we determined the photon flux using standard ferrioxalate actinometer. The detail procedure is described in previous studies[3-5]. We irradiated 2 ml of 0.08 mol/L of freshly prepared ferrioxalate aqueous solution for 15 min by an 415 nm LED under the same illumination conditions that were utilized in the photocatalytic studies. After that, 2 ml of 0.08 mol/L of ferrioxalate were diluted with 25 mL of H_2O. 2 mL of the diluted solution were futher mixed with 5 mL of o-phenanthroline solution in DI water (1g/L), 5 ml of buffer solution prepared by mixing 36 ml of H_2SO_4 (1 mol/L), 60 mL of sodium acetate (1 mol/L) and 100 mL of DI water and finally 5 mL of DI water obtaining 17 mL of solution in total. This procedure resulted in a dilution of the initial sample by 114.75 times. The exposure of light sensitive chemicals (ferrioxalate) was minimized by wrapping the glassware with aluminum foil. The mixtures was left in the darkness for 30 minutes and after which the UV/Vis spectrum was recorded. A control sample (unexposed to LED light) underwent the same dilution/mixing procedures as the irradiated sample. The absorbance of $[Fe(II)(phen)_3]^{2+}$ at 510 nm of the irradiated sample and the control sample were 2.325 and 0.029, respectively.

The concentration change of the reduced Fe^{2+} was evaluated using formula (1)

$$\frac{n[Fe(phen)_3]^{\mathrm{II}}}{dt} = \frac{dAbs_{510}}{dt}\frac{V}{\varepsilon_{510} l} \qquad (1)$$

V = volume of solution irradiated, (2mL)
ε_{510} = molar extinction coefficient at 510 nm of $[Fe(phen)_3]^{2+}$ (11100 $M^{-1}cm^{-1}$)
l = pathlength (cm) (cuvette pathlength is 1 cm)

$$\mathrm{I}_0 dt = \frac{n[Fe(phen)_3]^{II}}{\Phi_{Fe^2,\lambda}} \qquad (2)$$

where I_0dt is incident photon flux and $\Phi_{Fe^2,\lambda}$ is quantum efficiency for ferrioxalate (~1.1) at wavelength close to 415 nm.[6] The photon flux of the original reaction mixture, after considering dilution factor , is 4.22×10^{-5} moles.

The apparent quantum yield was calculated using formula (3).

$$\Phi_{\mathrm{X}_i} \equiv \frac{d[X_i]}{I_0 dt} \qquad (3)$$

The conversion of thiophenol (0.2 mmol in 2 mL) after 15 min was 11%, which is equivalent to $d[X_i]$ =2.2×10^{-5}mol. So the APY of our reaction is ~52%.

3. EPR Analysis

The direct detection of the $OO^{-\bullet}$ by EPR spectroscopy is challenging. First, $OO^{-\bullet}$ is very reactive and hence, it is not possible to reach its concentration detectable by EPR. Second, the free $OO^{-\bullet}$ the lowest energy state has a 2-fold orbital degeneracy. This coupling leads to a very strong dependence of the g-factor of the $OO^{-\bullet}$ ion on the orientation in the magnetic field. If the O-O axis is oriented parallel to the external field, the g-factor should be g_{par}= 4 and for perpendicular orientation g_{per}= 0. This leads to a considerable decrease of the EPR signal intensity under the detection limit. The direct detection by EPR spectroscopy is only possible if the $OO^{-\bullet}$ is in a lattice, bound at a solid surface. In liquids, the detection of $OO^{-\bullet}$ is only possible after a reaction with a second compound. Usually nitrones were used for this purpose. These nitrones are well-known as spin traps. The result of the trap reaction is the so-called spin adduct. That means a new covalent bond between the $OO^{-\bullet}$ and the spin trap is formed, and the spin adduct is detected by EPR spectroscopy and not the $OO^{-\bullet}$. This method is not unequivocal. It is known that nitrones are susceptible to a nucleophilic addition of water. The following oxidation by mild oxidants, e.g., small amounts of oxygen, will produce the same compound as formed in the case of trapping a hydroxyl radical.[7]

4. Band Alignment of CdSe/CdS Heterostructures

Our synthesis yield wurtzite structure for both CdSe seed and CdS shell. Because the length of CdS nanorod is relatively long (~28nm) and the nanorod is only confined in the radial direction, we do not expect the band position of CdS to deviate significantly from the bulk value.[8, 9] The optical absorbance data shown in Figure 1a, shows the band gap of CdS is 2.53eV, only slightly larger than 2.50eV of the bulk value.[9, 10] Thus, we used the band position of the bulk value adjusted for NHE, with valence band edge at +1.73V and conductive band at -0.77V.[10] The valence band offset between CdSe and CdS is relatively well established in the literature. We use the value of 0.39V obtained through local density approximation calculation, [11] which put the valence band edge of CdSe at +1.34V. The measured band gap in our CdSe seed is 2.03eV, which put the conduction band edge of CdSe at -0.69V. So the conduction band edge difference between CdSe and CdS will be 0.08V, or if we used band gap of measured CdS of 2.53V, the band edge offset would be 0.11V. The position assigned here for 3.1nm CdSe core is consistent with data obtained through cyclic voltammetry measurements, within the error bar obtained from measurements from different groups.[12]

Although the illustrated band structure (Fig. 4b) of the CdSe/CdS core-shell system is type-I, the conduction band edge offset is very small, so the photoexcited electron can delocalized into the CdS nanorod at room temperature (a so-called quasi-type II band alignment). The delocalization of photoexcited electron depends also on the size of CdSe core and the excitation energy, which has been confirmed in a separate time-dependent photoluminescence and transient absorption study of similar samples synthesized in our lab [13, 14] and independently by others.[15] This band alignment structure is also consistent with the temperature dependent electron delocalization phenomenon observed in CdSe/CdS core-shell structure.[16]

5. Redox Potential of the Thiophenol and Corresponding Thiolate and Oxygen in Organic Solvents

No electrochemical data are available for toluene solution. Typically, electrochemical studies in organic solvents are conducted in acetonitrile (MeCN) and dimethylformamide (DMF). The positions of the redox potentials of thiophenol and its thiolate form were calculated against normal hydrogen electrode (NHE) using data reported in Ref.[17, 18] where the redox potentials of thiophenol and its thiolate form were measured in organic solvents (acetonitrile, MeCN) using the internal redox electrode such as ferrocene/ferrocenium (Fc/Fc^+). [18] Note, that there are some discrepancies in the values of redox potential for ferrocene/ferrocenium redox couple reported by different groups. For instance, $E(Fc/Fc^+)$ vs SCE was reported as 0.48 V and 0.47 V in MeCN and DMF, respectively,[17] 0.47 V in DMF vs NHE,[19] 0.272 V in MeCN vs Ag/AgCl,[20] 0.403 V vs SCE in MeCN[21] and 0.875 V vs Ag/AgI reference electrode.[18] Also the peak positions corresponding to redox processes depend on the solvent and concentration of additives.[17] The potentials of $E(H_2O/O_2)$ and $E(H_2/H^+)$ in MeCN and DMF were reported in Ref.[22] To recalculate the redox potentials for O2/H2O vs NHE, we used data for $E(Fc/Fc^+)$ provided in Ref[17] since this study reports the most detailed analysis of electrochemical oxidation of ferrocene in different solvents (bottom boundary of the broad lines show in in Fig. 4b). However, we also added to Figure 4b the values of redox potential normalized by the $E(Fc/Fc^+)$ reported by other authors. All potentials plotted in Figure 4b were converted into potentials vs normal hydrogen electrode (NHE). [19-21]

6. Discussion on the possibility of ROS formation during oxygen reduction reaction by photo excited electrons.

Previous studies have shown that four electron process that leads to H_2O formation is a thermodynamically more favorable process as compared to two electron process responsible for H_2O_2 formation.[23] The formation of H_2O_2 as a result of electron transfer has been observed for CdSe/CdS NRs in aqueous media.[24] The previous data indicated that H_2O_2 can oxidize both neutral thiol and thiolate into disulfide, as well as generate other side products of overoxidation, such as sulfenic acid (RSOH), sulfinic acid (RSO_2H), sulfonic acid (RSO_3H) or their deprotonated forms.[25, 26] These side products have not been detected in our photocatalytic reaction. To further test whether H_2O_2 generation plays a role in thiol coupling chemistry in organic solvent, we conducted control experiments with adding aqueous H_2O_2 to the reaction media in toluene. With no CdSe/CdS NRs, addition of H_2O_2 converted thiolate into disulfide nearly 100% yield with no other side product detected. In comparison, there was ~0% conversion of thiol by H_2O_2. However, in the presence of CdSe/CdS NRs, even with H_2O_2 added at ~1/5 of the concentration of thiophenol, there was nearly immediate degradation of NRs, as it is evident by the UV-Vis spectra (Fig. S4). We observed that CdSe/CdS NRs in the presence of thiophenol were more stable. However, both CdSe/CdS NRs solution and the solution consisting of CdSe/CdS NRs, thiophenol and amine completely degraded after 1 h of addition of H_2O_2. More importantly, it is worth noting that in the case of thiolate, the degradation of NRs occurs almost immediately (within 3 minutes, even before the sample was exposed to blue light). Thus, the presence of thiolate makes CdSe/CdS NRs more vulnerable for oxidation, even though thiolate itself is highly oxidizable by H_2O_2.[27, 28] Considering the partition coefficient of H_2O_2 in organic solvent is very low,[29] the actual

contributing H_2O_2 in toluene is much lower than the concentration we added. Since in our photocatalytic reaction, the CdSe/CdS NRs are much more stable and do not degrade completely even after 4 photocatalytic cycles (equivalent of 8 h of reaction with exposure to 415 nm light), we conclude that the presence of reactive oxygen species, such as H_2O_2, is very low. The formation of H_2O, a thermodynamically favorable product, is the most likely process responsible for electron transfer. Previous studies have also shown the formation of H_2O vs H_2O_2 is determined by the adsorption mode of O_2 molecule and the intermediate species formed on the surface.[30, 31] If O_2 molecule lands "flat" on the catalytic surface, it dissociates into two oxygen atoms that form H_2O upon their interactions with protons. In turn, when O_2 interacts with the catalytic via side, it adsorbs the electron and reaction pathway responsible for the formation of H_2O_2 is tuned. It is reasonable to suggest that surface chemistry influences the adsorption mode of O_2 that, in turn, explains the difference of the products photosynthesized by electron transfer to O_2 in water and toluene that we used in our study.

Control experiment 1. Test the effect of hydrogen peroxide on the oxidation of thiol and thiolate in toluene

Reaction Conditions	Product detected by GC-MS
Thiophenol in toluene under air with blue LED.	No reaction product formed
Thiophenol + H_2O_2 in toluene with blue LED	No reaction product formed
Thiophenol + amine + H_2O_2 in toluene with blue LED	Disulfide detected with nearly 100% conversion

*The reaction condition is as follows, thiophenol (0.2 mmol), *n*-octylamine (0.2 mmol), and toluene (2.0 mL) under 415 nm blue LED light and air at room temperature. 30% aqueous solution of H_2O_2 was added with H_2O_2 is at 0.2mmol. The reaction yield was determined by GC-MS using biphenyl as an internal standard.

Control experiment 2.

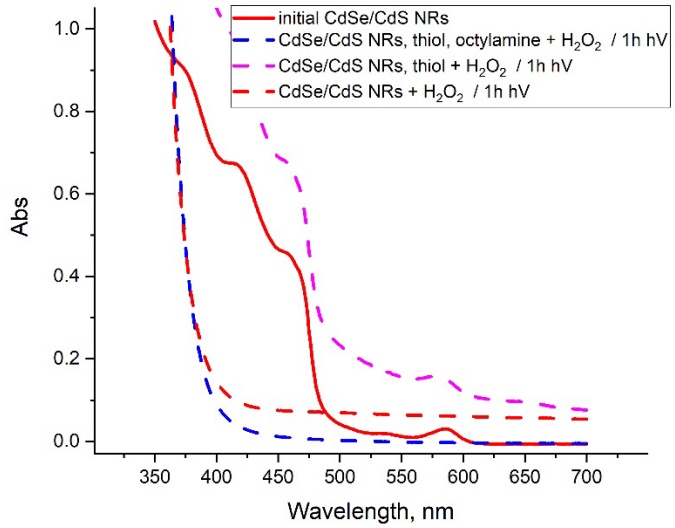

Fig. S4. The evolution of the UV/Vis spectra of CdSe/CdS NRs dissolved in toluene after addition of H_2O_2 and 1 h exposure to the light at 415 nm at room temperature. The amount of peroxide was ~1/5 of the amount of thiophenol. The background elevation due to scattering is a result of the emulsion formation since the water solution of H_2O_2 was used. It is most pronounced in the case of CdSe/CdS NRs and thiophenol sample. The UV/Vis data indicate the complete degradation of CdSe/CdS NRs initiated by addition of H_2O_2. Importantly, in the case CdSe/CdSe NRs with added thiophenol and amine the degradation takes place within 3 min after addition of H_2O_2. Note, that spectra of CdSe/CdS NRs with added thiophenol was similar to those of CdSe/CdSe with thiophenol and octylamine and CdSe/CdS also indicating the degradation of NRs.

1. D. V. Talapin, J. H. Nelson, E. V. Shevchenko, S. Aloni, B. Sadtler and A. P. Alivisatos, *Nano Letters*, 2007, **7**, 2951-2959.
2. L. Carbone, C. Nobile, M. De Giorgi, F. D. Sala, G. Morello, P. Pompa, M. Hytch, E. Snoeck, A. Fiore, I. R. Franchini, M. Nadasan, A. F. Silvestre, L. Chiodo, S. Kudera, R. Cingolani, R. Krahne and L. Manna, *Nano Letters*, 2007, **7**, 2942-2950.
3. T. Aillet, K. Loubiere, O. Dechy-Cabaret and L. Prat, *International Journal of Chemical Reactor Engineering*, 2014, **12**, 257-269.
4. M. R. Hoffmann, S. T. Martin, W. Choi and D. W. Bahnemann, *Chemical Reviews*, 1995, **95**, 69-96.
5. J. Comerford, Investigation of photochemical reactions using the Cary 50/60 UV-Vis, https://www.agilent.com/cs/library/applications/uv76.pdf).
6. C. G. Hatchard, C. A. Parker and E. J. Bowen, *Proceedings of the Royal Society of London. Series A. Mathematical and Physical Sciences*, 1956, **235**, 518-536.
7. R. Nishiyabu and P. Anzenbacher, *Journal of the American Chemical Society*, 2005, **127**, 8270-8271.
8. H.-W. Tseng, M. B. Wilker, N. H. Damrauer and G. Dukovic, *Journal of the American Chemical Society*, 2013, **135**, 3383-3386.
9. L. Brus, *The Journal of Physical Chemistry*, 1986, **90**, 2555-2560.
10. C. G. Van de Walle and J. Neugebauer, *Nature*, 2003, **423**, 626-628.
11. J. Li and L.-W. Wang, *Applied Physics Letters*, 2004, **84**, 3648-3650.
12. P. P. Ingole, *Physical Chemistry Chemical Physics*, 2019, **21**, 4695-4716.
13. C. She, A. Demortière, E. V. Shevchenko and M. Pelton, *The Journal of Physical Chemistry Letters*, 2011, **2**, 1469-1475.
14. C. She, G. W. Bryant, A. Demortière, E. V. Shevchenko and M. Pelton, *Physical Review B*, 2013, **87**, 155427.
15. G. Rainò, T. Stöferle, I. Moreels, R. Gomes, J. S. Kamal, Z. Hens and R. F. Mahrt, *ACS Nano*, 2011, **5**, 4031-4036.
16. B. Kundu, S. Chakrabarti and A. J. Pal, *Journal of Applied Physics*, 2016, **119**, 104304.
17. D. Bao, B. Millare, W. Xia, B. G. Steyer, A. A. Gerasimenko, A. Ferreira, A. Contreras and V. I. Vullev, *The Journal of Physical Chemistry A*, 2009, **113**, 1259-1267.
18. F. G. Bordwell, X.-M. Zhang, A. V. Satish and J. P. Cheng, *Journal of the American Chemical Society*, 1994, **116**, 6605-6610.
19. S. K. Haram, B. M. Quinn and A. J. Bard, *Journal of the American Chemical Society*, 2001, **123**, 8860-8861.
20. W. Hong, B. Sun, H. Aziz, W.-T. Park, Y.-Y. Noh and Y. Li, *Chemical Communications*, 2012, **48**, 8413-8415.
21. A. Paul, R. Borrelli, H. Bouyanfif, S. Gottis and F. Sauvage, *ACS Omega*, 2019, **4**, 14780-14789.

22. M. L. Pegis, J. A. S. Roberts, D. J. Wasylenko, E. A. Mader, A. M. Appel and J. M. Mayer, *Inorganic Chemistry*, 2015, **54**, 11883-11888.
23. S. Siahrostami, G.-L. Li, V. Viswanathan and J. K. Nørskov, *The Journal of Physical Chemistry Letters*, 2017, **8**, 1157-1160.
24. N. Waiskopf, Y. Ben-Shahar, M. Galchenko, I. Carmel, G. Moshitzky, H. Soreq and U. Banin, *Nano Letters*, 2016, **16**, 4266-4273.
25. L. A. H. van Bergen, G. Roos and F. De Proft, *The Journal of Physical Chemistry A*, 2014, **118**, 6078-6084.
26. A. Zeida, R. Babbush, M. C. González Lebrero, M. Trujillo, R. Radi and D. A. Estrin, *Chemical Research in Toxicology*, 2012, **25**, 741-746.
27. A. A. Oswald, F. Noel and A. J. Stephenson, *The Journal of Organic Chemistry*, 1961, **26**, 3969-3974.
28. T. J. Wallace, N. Jacobson and A. Schriesheim, *Nature*, 1964, **201**, 609-610.
29. J. H. Walton and H. A. Lewis, *Journal of the American Chemical Society*, 1916, **38**, 633-638.
30. D. W. Flaherty, *ACS Catalysis*, 2018, **8**, 1520-1527.
31. Z. Lu, G. Chen, S. Siahrostami, Z. Chen, K. Liu, J. Xie, L. Liao, T. Wu, D. Lin, Y. Liu, T. F. Jaramillo, J. K. Nørskov and Y. Cui, *Nature Catalysis*, 2018, **1**, 156-162.